Supporting Information

High Yield Regeneration of 1,4-NAD(P)H by Selective Ad/De-sorption-Mediated Visible-Light Photocatalysis on a Noble-Metal-Free Catalyst

Zheng-Wu Wang,[‡a] Xin Tan,[‡a] Zheng-Hao Wu,[a] Jun-Hao Chen,[a] Yi-Zhou Zhu,*[b] and He-Fang Wang*[a]

Zheng-Wu Wang, Xin Tan, Zheng-Hao Wu, Jun-Hao Chen and He-Fang Wang

Research Center for Analytical Sciences, College of Chemistry, Nankai University, Tianjin Key Laboratory of Biosensing and Molecular Recognition, Tianjin, 300071, China

E-mail: wanghefang@nankai.edu.cn

Yi-Zhou Zhu

State Key Laboratory and Institute of Elemento-Organic Chemistry, Nankai University, Tianjin, 300071, China

E-mail: zhuyizhou@nankai.edu.cn

1. Experimental section

1.1 Reagents

$Al(NO_3)_3 \cdot 9H_2O$, $AlCl_3$ and triethanolamine (TEOA) were purchased from Aladdin (Shanghai, China). Urea (99%) were purchased from Shanghai Macklin Biochemical Co., Ltd (Shanghai, China). Wahaha pure water was used in this work. $BiCl_3$, $Bi(NO_3)_3 \cdot 5H_2O$, β-Nicotinamide adenine dinucleotide (NAD^+, 97%), reduced coenzyme I (β-NADH, 98%), β-Nnicotinamide adenine dinucleotide phosphate (β-$NADP^+$, 95%), and reduced coenzyme II (β-NADPH, 97%) were purchased from Heowns Biochemical Technology Co., Ltd (Tianjin, China). Alcohol dehydrogenase (ADH, 99%) was purchased from KeyGEN Bio TECH (Jiangsu, China). HCl and HNO_3 were from Bohua Chemical Reagent Co., Ltd (Tianjin, China). Benzylamine and *N*-benzylbenzaldimine were from Meryer (Shanghai, China).

1.2 Apparatus

The X-ray powder diffraction (XRD) patterns were recorded using a Rigaku D/max-2500 X-ray diffractometer (Rigaku, Japan). Morphology and microstructure were characterized via high resolution transmission electron microscopy (HRTEM) using a Talos F200X G2 high-resolution transmission electron microscope (FEI, Czech) operating at a 200 kV accelerating voltage. The UV–vis diffuse reflection spectra (DRS) with $BaSO_4$ as a reference and the UV-vis absorption spectra of all aqueous solutions were measured on a UV–vis spectrophotometer (UV-2600, Shimadzu, Japan). The photocurrent measurements were carried out using an electrochemical workstation (Zahner, Germany) equipped with standard three electrodes (an appropriate amount of the sample suspension on a conductive indium tin oxide glass, a standard saturated calomel electrode (SCE) as reference electrode, and platinum as the counter electrode). A 0.5 $mol \cdot L^{-1}$ Na_2SO_4 aqueous solution was used as the electrolyte. The Brunauer-Emmett-Teller (BET) method was employed to determine specific surface area, utilizing a Micromeritics ASAP 2460 specific surface area analyzer (Micromeritics, US). X-ray photoelectron spectroscopy (XPS) tests were performed on an Axis Ultra DLD X-ray photoelectron spectrometer (Kratos Analytical Ltd, UK). ^1H NMR spectra were recorded on a Bruker AC-400 FT (400 MHz). High-performance liquid chromatography (HPLC, Waters 2695 with a C18 column) was used for analysis of the products from photocatalytic NAD^+ reduction and benzylamine oxidation.

1.3 Synthesis of $Bi_{12}O_{17}Cl_2$-$Bi_{48}Al_2O_{75}$-Al_2O_3, $Bi_{12}O_{17}Cl_2$-Al_2O_3, and $Bi_{48}Al_2O_{75}$-Al_2O_3.

A certain amount of $BiCl_3$, $Al(NO_3)_3 \cdot 9H_2O$, urea and 100 mL purified water were weighed in a beaker. After ultrasonic treatment, the mixture was stirred at room temperature for 30 min, and then the mixture was transferred into Teflon linear autoclave and heated at 125 ℃ for 15 h. The reaction vessels were taken out and cooled to room temperature, and then the mixture was transferred to 50 mL centrifuge tubes, the solid was harvested and washed with pure water twice and ethanol once, and then was dried at 60 ℃ to obtain the precursors. Finally, the precursors were calcined at 450 ℃ in Muffle furnace for 4 h to get $Bi_{12}O_{17}Cl_2$-$Bi_{48}Al_2O_{75}$-Al_2O_3. The feeding ratios of $Al(NO_3)_3 \cdot 9H_2O/BiCl_3$ (1/9, 3/7, 5/5, 7/3 and 9/1) and urea/$BiCl_3$ (2/1, 8/1, 16/1 and 32/1) and hydrothermal temperature (70, 90,125 and 155 ^oC) were changed to research the best condition to get the best $Bi_{12}O_{17}Cl_2$-$Bi_{48}Al_2O_{75}$-Al_2O_3 photocatalyst. For synthesis of $Bi_{12}O_{17}Cl_2$-Al_2O_3, the anhydrous $AlCl_3$ instead of $Al(NO_3)_3 \cdot 9H_2O$ was used. For synthesis of $Bi_{48}Al_2O_{75}$-Al_2O_3, $Bi(NO_3) \cdot 5H_2O$ instead of $BiCl_3$ was used. Other synthetic operations were the same as the preparation of $Bi_{12}O_{17}Cl_2$-$Bi_{48}Al_2O_{75}$-Al_2O_3.

1.4 Determination of composition content of $Bi_{12}O_{17}Cl_2$-$Bi_{48}Al_2O_{75}$-Al_2O_3.

The composition content in $Bi_{12}O_{17}Cl_2$-$Bi_{48}Al_2O_{75}$-Al_2O_3 was determined by measuring the Cl^- content in the supernatant after the hydrothermal reactions. For the determination of Cl^-, 1 mL of supernatant was mixed with 19 mL of H_2O and 1 mL of 0.053 M $K_2Cr_2O_7$. Then, the pH was adjusted to 7 using 1 M of HNO_3 solution. The $AgNO_3$ solution of 0.0105 M was added into mixture until the brick red precipitate appeared. The concentration of Cl^- in the supernatant was calculated based on volume of $AgNO_3$ solution. The $Bi_{12}O_{17}Cl_2$ content was calculated from Cl in the solid (total feeding of Cl minuses Cl in the supernatant), and $Bi_{48}Al_2O_{75}$ content was calculated from Bi (total Bi minuses Bi in $Bi_{12}O_{17}Cl_2$), and Al_2O_3 content was from Al (total Al minuses Al in $Bi_{48}Al_2O_{75}$).

1.5 Visible light photocatalytic regeneration of NADH with TEOA as sacrificial agent

An aqueous dispersion of photocatalyst (1.5 $g \cdot L^{-1}$), TEOA (0.5 M) and NAD^+ (0.3 mM) was added into the quartz reactor, and ultrasonically treated for 10 min. The dispersion was then exposed to a 20 W LED lamp (λ=455 nm). 3 mL of suspension was sucked out from the quartz tube at different time intervals (20, 40, 60, 90 min). The supernatants acquired by filtration of the suspensions with 0.22 μm filters were measured by the UV-vis absorption spectrometry or HPLC chromatography for determination of NADH concentration (C_{NADH}). Additionally, ^1H

NMR spectra was recorded to identify 1,4-NADH. The yield of NADH was calculated according to the eq. 1.

$$\text{Yield of NADH (\%)} = \frac{C_{NADH}}{C_{NAD^+}} \times 100\% \quad (1)$$

where C_{NAD^+} was the initial concentration of NAD^+ (0.2 $g \cdot L^{-1}$ is equivalent to 0.3 mM).

1.6 Coupling photocatalytic reduction of NAD^+ with oxidation of benzylamine

An aqueous dispersion of photocatalyst (1.5 $g \cdot L^{-1}$), benzylamine (5 mM) and NAD^+ (0.3 mM) were added to the quartz reactor, and then ultrasonically treated for 10 min. The dispersion was exposed to a 20 W LED lamp (λ=455 nm). 3 mL of suspensions were sucked out from the quartz tube at different time intervals, and the supernatants acquired by filtration of the liquid phase with 0.22 μm filters were detected by HPLC. The yield of NADH and *N*-benzylbenzaldimine was calculated according to standard curves.

1.7 Determination of the selectivity of 1,4-NADH

The reaction for biocatalytic consuming the biologically active 1,4-NADH was used to measure the selectivity of 1,4-NADH. ADH (2 $g \cdot L^{-1}$, 1.5 KU) and acetaldehyde (100 μL) were added to the supernatant from the photocatalytic regeneration of NADH in **1.5** or **1.6** for certain durations. The concentration of biologically active 1,4-NADH ($C_{1,4\text{-}NADH}$) was calculated according to the following eq. 2:

$$C_{1,4\text{-}NADH} = C_{\text{NADH-photocatalysis}} - C_{\text{NADH-after bio-catalysis}} \quad (2)$$

where $C_{1,4\text{-}NADH}$ was the concentration of biologically active 1,4-NADH ($g \cdot L^{-1}$) after biocatalysis reaction, $C_{\text{NADH-photocatalysis}}$ was the concentration of total regenerated NADH measured in photocatalysis process. $C_{\text{NADH-after bio-catalysis}}$ was the concentration of residual non-biologically active NADH measured after bio-catalysis process with ADH and acetaldehyde added.

The selectivity of 1,4-NADH was calculated according to eq. 3:

$$\text{selectivity of 1,4-NADH (\%)} = \frac{C_{1,4-NADH}}{C_{NADH-photocatalysis}} \quad (3)$$

The selectivity of 1,4-NADPH was determined according to the same procedure as 1,4-NADH.

1.8 Measurement of adsorption of NAD^+ on photocatalyst

The adsorption experiments of NAD^+ on photocatalyst were the same as **1.5** except without TEOA and light illumination, and the suspensions were kept in the dark. The supernatant was diluted threefold and measured by UV-2600 ultraviolet-visible spectrometer.

1.9 Desorption of unreacted NAD^+ after photocatalytic reaction

The eluent of 0.1 M pH~13 was prepared with NaOH for use. After the photocatalytic experiment, the photocatalyst after centrifugation was collected, and then the same volume of eluent as the photocatalytic experiment was added. The resultant dispersion was ultrasonicated for 60 min, and then the supernatant was diluted threefold and measured by UV-2600 ultraviolet-visible spectrometer. The concentration of NAD^+ desorbed from $Bi_{12}O_{17}Cl_2$-$Bi_{48}Al_2O_{75}$-Al_2O_3 was calculated according to the calibration curve of NAD^+ and listed in Table S2.

1.10 Successive use of $Bi_{12}O_{17}Cl_2$-$Bi_{48}Al_2O_{75}$-Al_2O_3 for regeneration of NADH

A typical photocatalytic reaction as **1.5** was carried out for 60 min (1 mL of reactants was piped out at 20, 40 and 60 min), and then 3 mL of fresh NAD^+ (0.3 mM) was added into the photocatalytic system. The above process was repeated again. For each repeat process, the NADH yield was calculated by subtraction of the NADH generated from last cycle from the total NADH.

1.11 DFT calculation of the adsorption energies.

The DFT calculations employed the Vienna ab initio simulation package(VASP 5.4.4),[1] where the PBE functional was utilized for exchange-correlation modeling,[2] and the projected augmented wave method described ion-electron interactions.[3] A 17.53×17.53×21.64 Å (90°×90°×90°, comprising 48 atoms of Al, 2 atoms of Bi, and 75 atoms of O) cell was constructed to simulate the adsorption of NAD^+ and NADH on the (001) facet of $Bi_{48}Al_2O_{75}$. In these simulations, atoms in the upper layer of the surface could move freely, while the bottom three layers (0.9 Å/layer) were fixed, and a 15 Å vacuum layer was utilized along the z-direction. The Monkhorst-Pack grid mesh-based Brillouin zone k-points were uniformly set at 1×1×1 for periodic structures, [4] and cutoff energy was set to 500 eV. Convergence criteria were set at 0.02 $eV \cdot Å^{-1}$ for force and 10^{-5} eV for energy.

The adsorption energy calculation of NAD^+ (E_{adsNAD^+}) and NADH ($E_{adsNADH}$) is based on eq. 4, 5:

$$E_{adsNAD^+} = E[*NAD^+] - E[NAD^+] - E^* \quad (4)$$

$$E_{adsNADH} = E[*NADH] - E[NADH] - E^* \quad (5)$$

E *, E [NAD^+], E [NADH], E [*NAD^+] and E [*NADH] represent the electronic energy of $Bi_{48}Al_2O_{75}$ (001) facet, NAD^+, NADH, NAD^+ adsorbed on $Bi_{48}Al_2O_{75}$ (001) facet and NADH adsorbed on $Bi_{48}Al_2O_{75}$ (001) facet, respectively.

2. Supporting figures and tables.

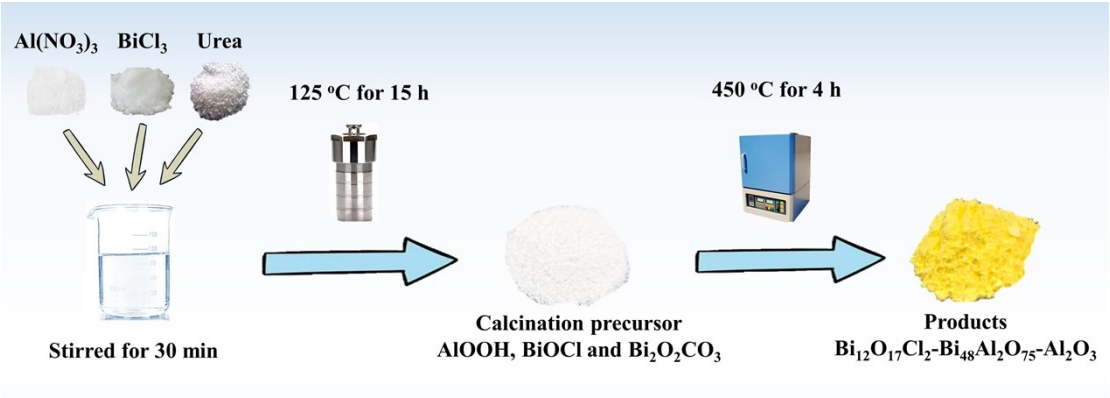

Fig. S1. Scheme illustration for preparation of the catalysts.

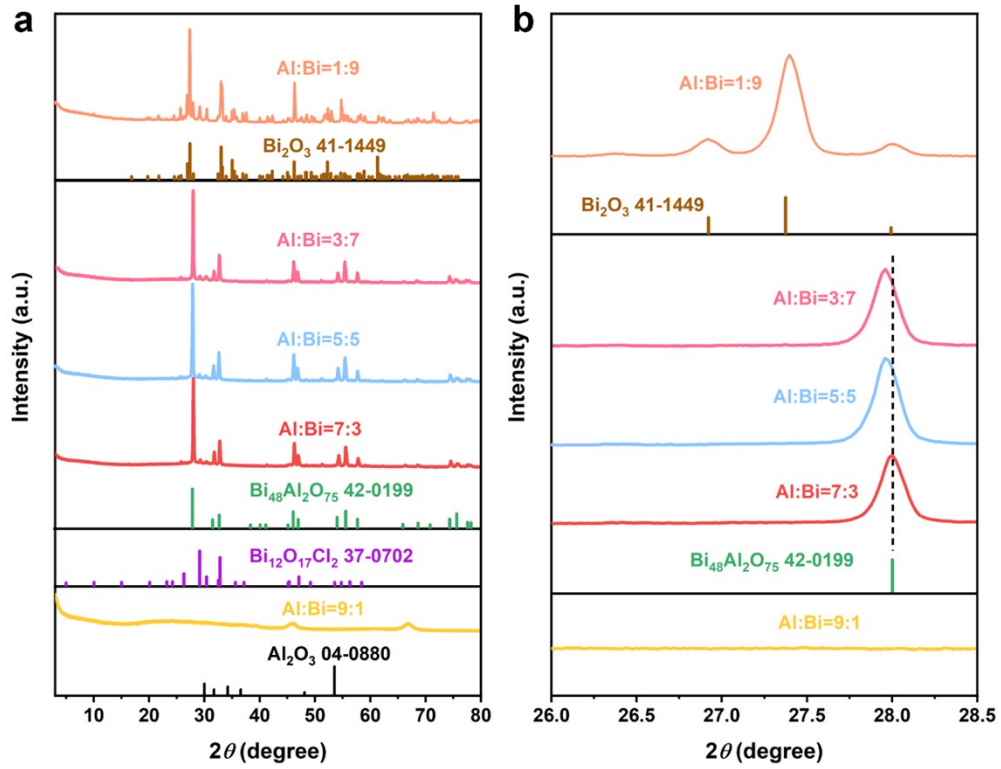

Fig. S2. (a) XRD patterns of the calcined products prepared with different mole ratios of Al:Bi of 1:9, 3:7, 5:5, 7:3, and 9:1; and (b) the partial enlarged details of 16-28.5 degree of (a).

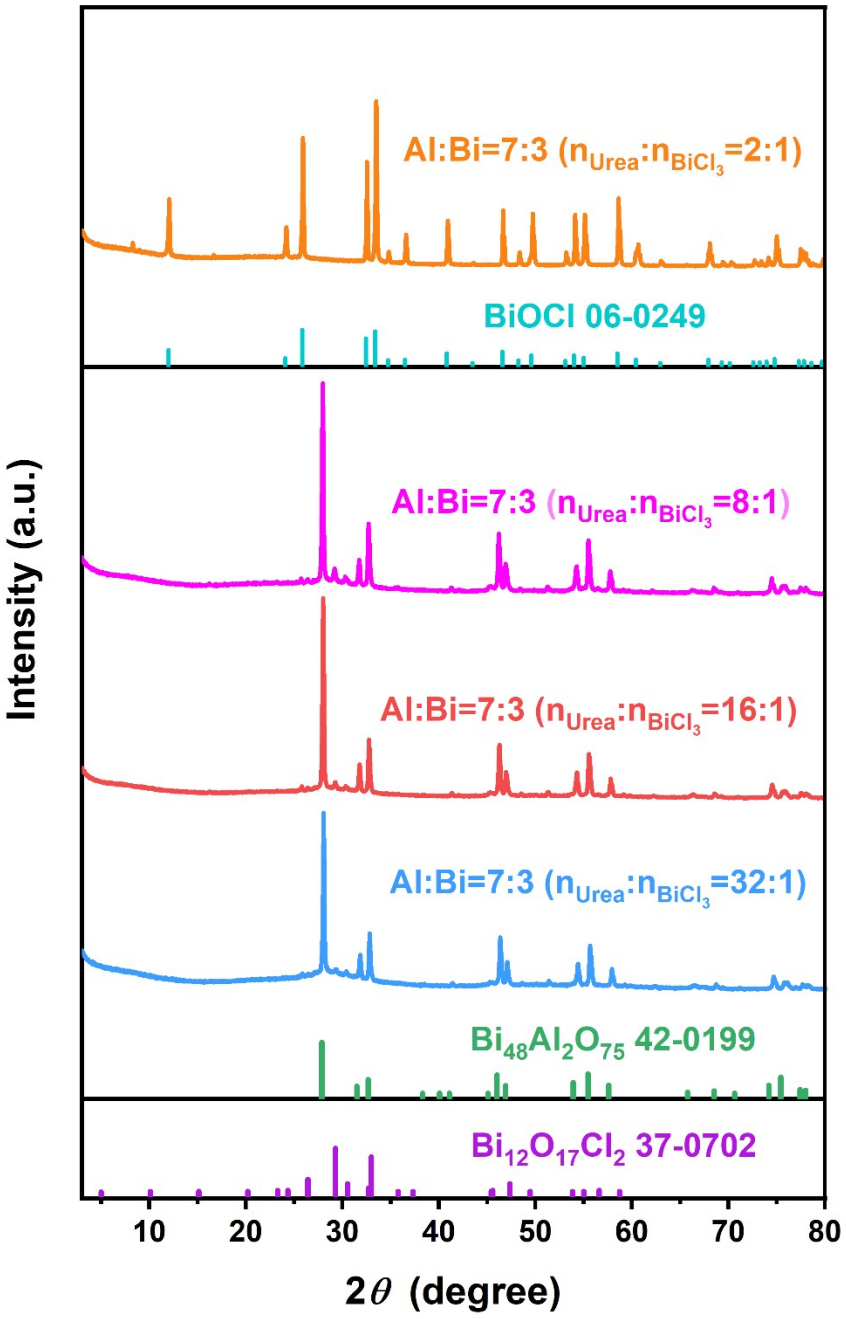

Fig. S3. XRD patterns of the calcined products prepared from Al:Bi set at 7:3 with different feeding mole ratio of urea:$BiCl_3$ of 2:1, 8:1, 16:1, and 32:1.

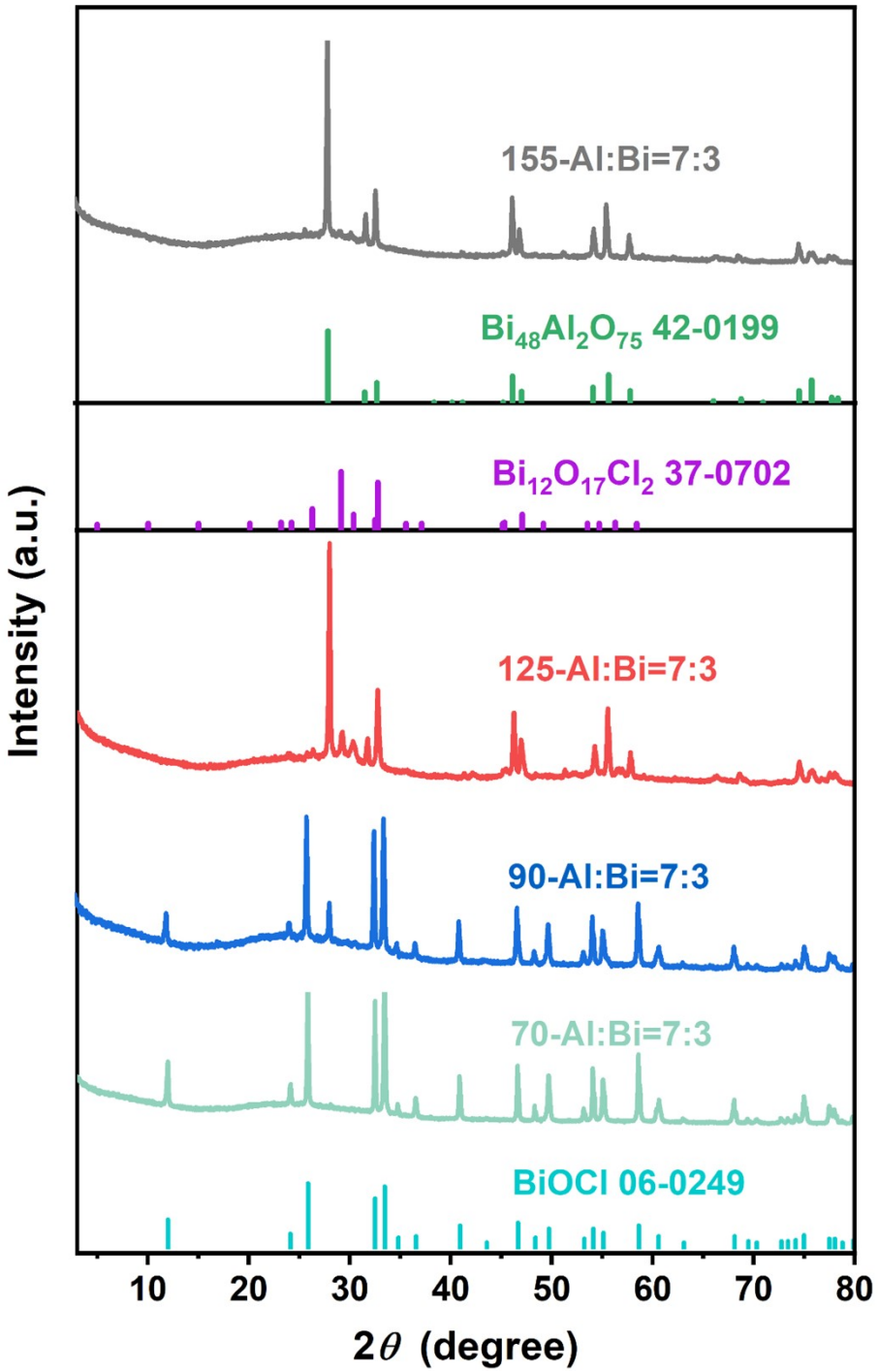

Fig. S4. XRD patterns of the calcined products prepared from Al:Bi set at 7:3 with different hydrothermal temperatures of 155, 125, 90 and 70 °C

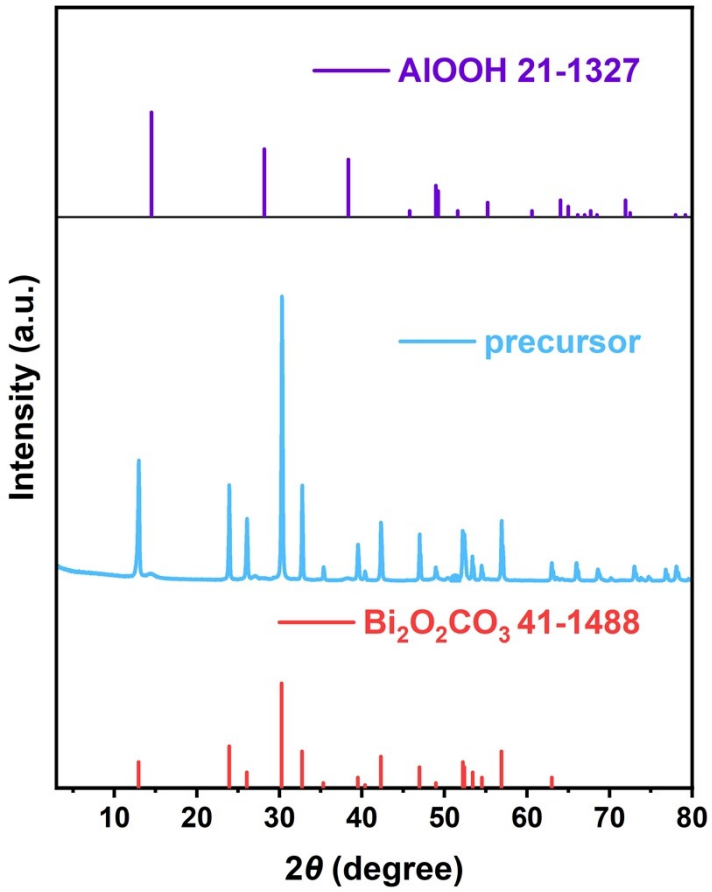

Fig. S5. XRD pattern of the calcination precursor acquired from feeding ratio of Al/Bi at 7/3 and urea/Bi at 16/1 and 125 °C hydrothermal temperature.

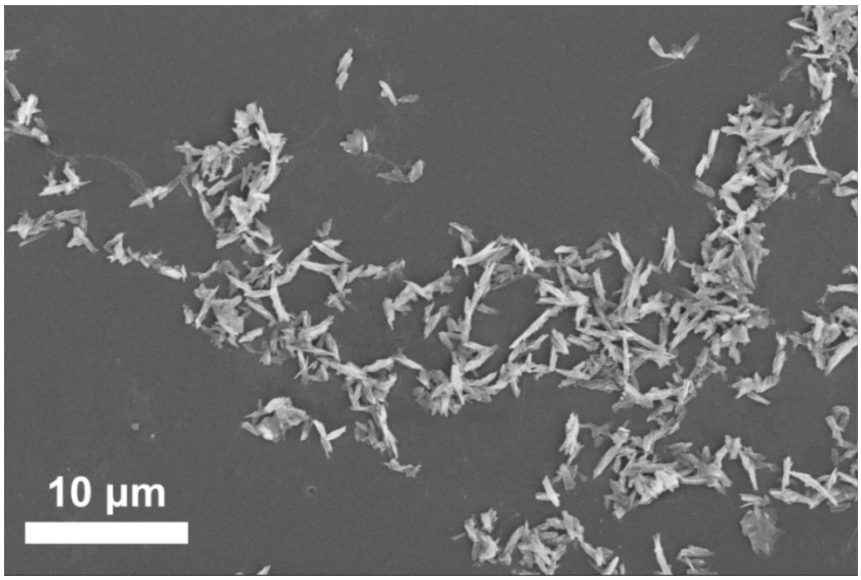

Fig. S6. SEM image of $Bi_{12}O_{17}Cl_2$-$Bi_{48}Al_2O_{75}$-Al_2O_3.

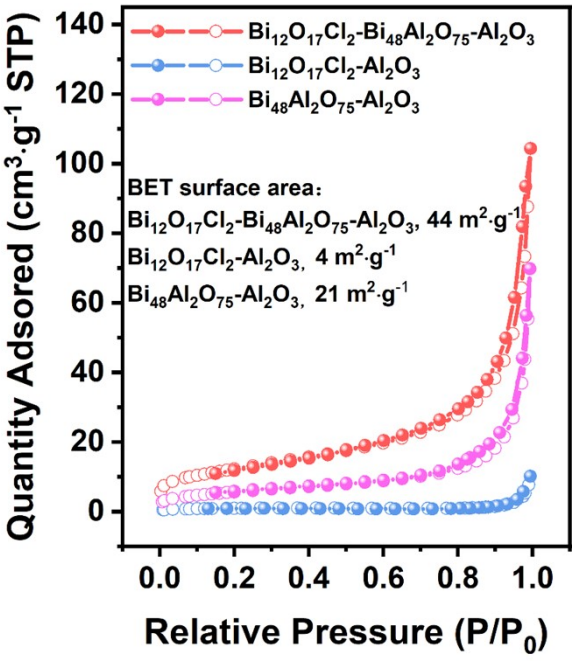

Fig. S7. N_2 adsorption-desorption isotherms of $Bi_{48}Al_2O_{75}$-Al_2O_3, $Bi_{12}O_{17}Cl_2$-$Bi_{48}Al_2O_{75}$-Al_2O_3, $Bi_{12}O_{17}Cl_2$-Al_2O_3.

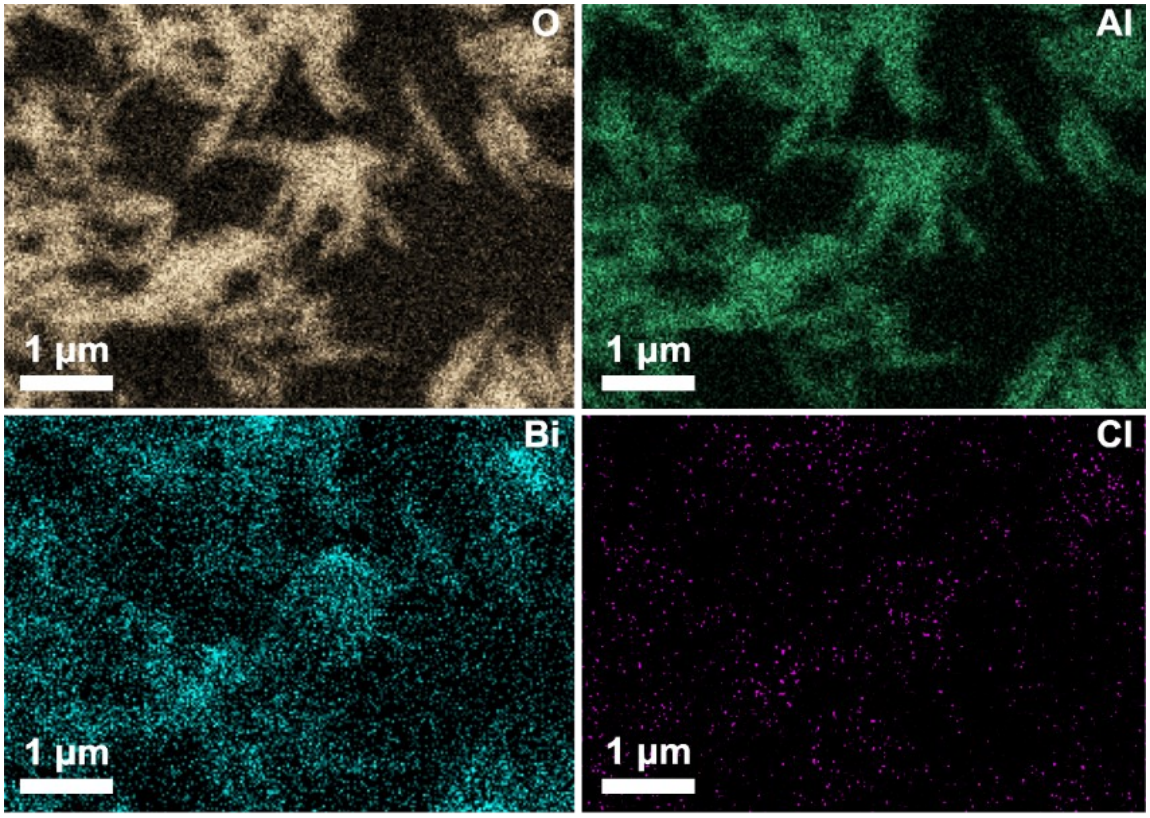

Fig. S8. The elemental mapping images of Al, Bi, O and Cl of $Bi_{12}O_{17}Cl_2$-$Bi_{48}Al_2O_{75}$-Al_2O_3.

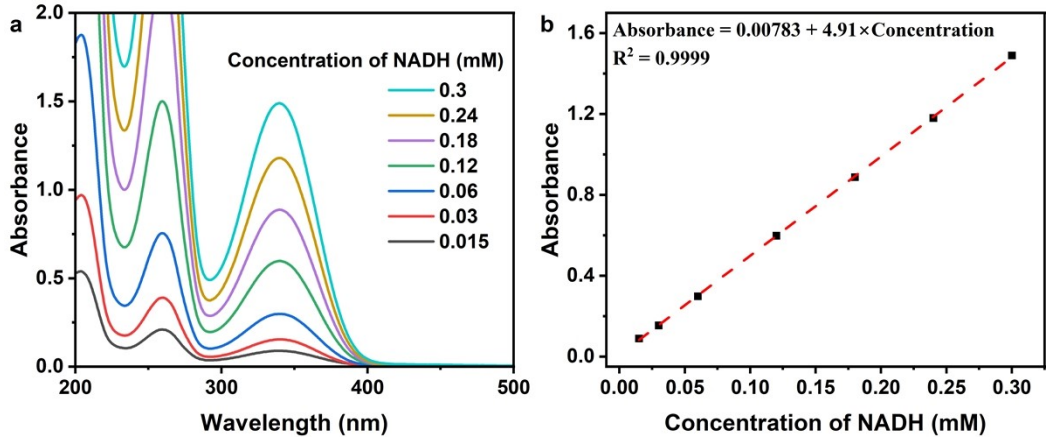

Fig. S9. Calibration with standard NADH solutions: (a) UV-Vis spectra of aqueous NADH solutions; (b) corresponding calibration curve derived from the absorbance at 340 nm in (a).

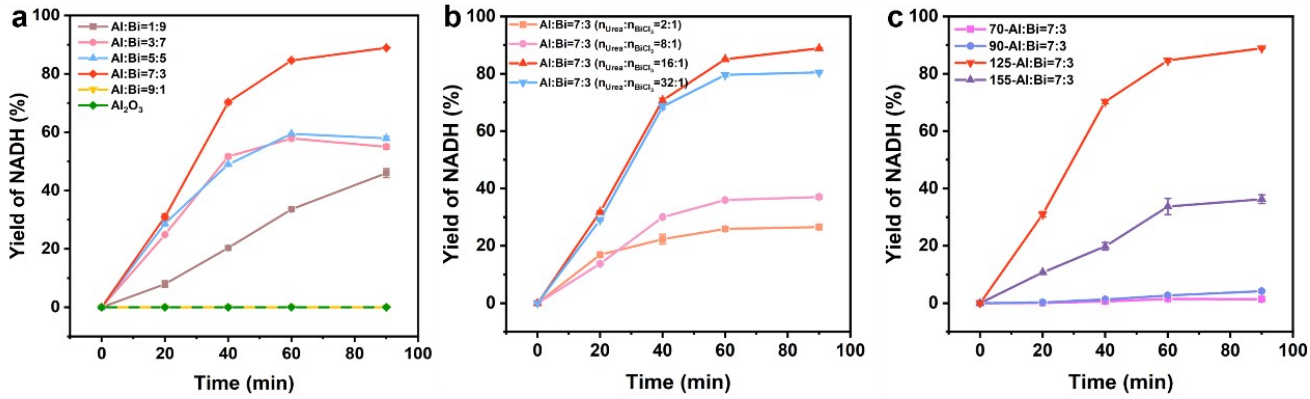

Fig. S10. The NADH yields of the catalysts prepared by 450 °C calcination of the precursors from different (a, b) feeding ratios of (a) Al/Bi, (b) urea/Bi and (c) temperature of the hydrothermal reactions.

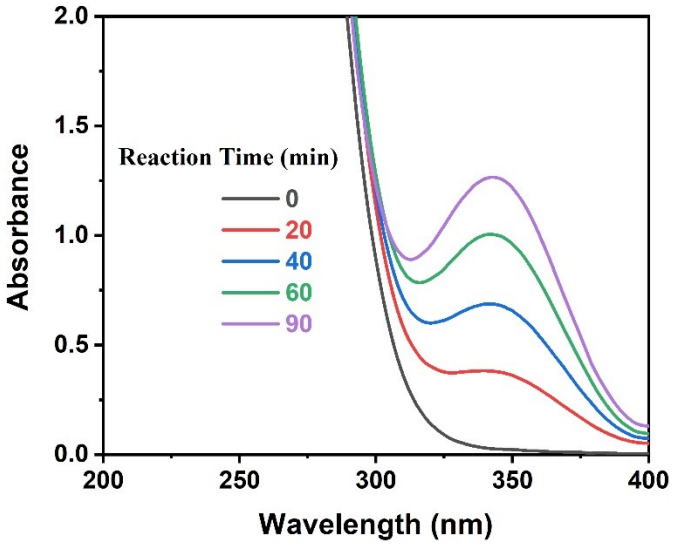

Fig. S11. UV-vis absorption spectra of photocatalytic regeneration of NADH at different time by $Bi_{12}O_{17}Cl_2$-$Bi_{48}Al_2O_{75}$-Al_2O_3 in the presence of TEOA.

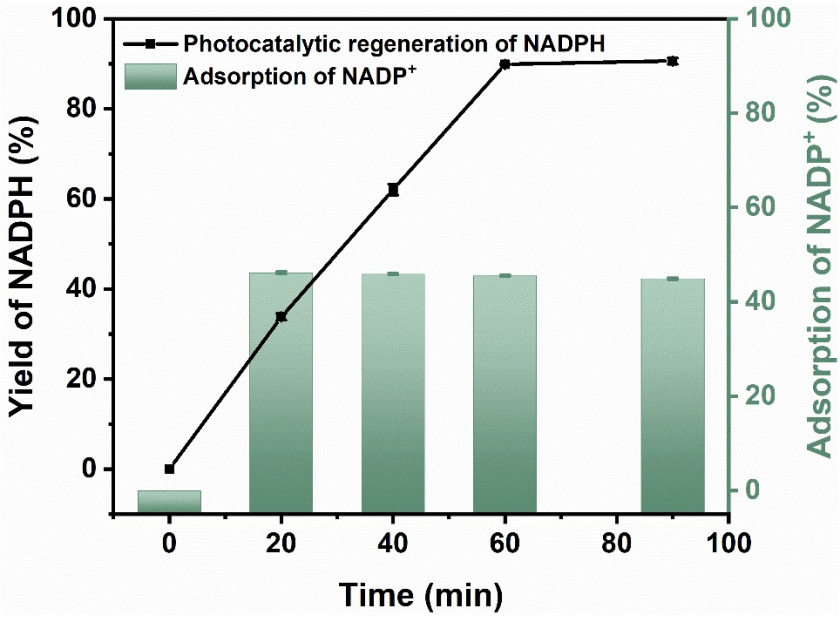

Fig. S12. The photocatalytic NADPH yields and $NADP^+$ adsorption at different time by $Bi_{12}O_{17}Cl_2$-$Bi_{48}Al_2O_{75}$-Al_2O_3 in the presence of TEOA.

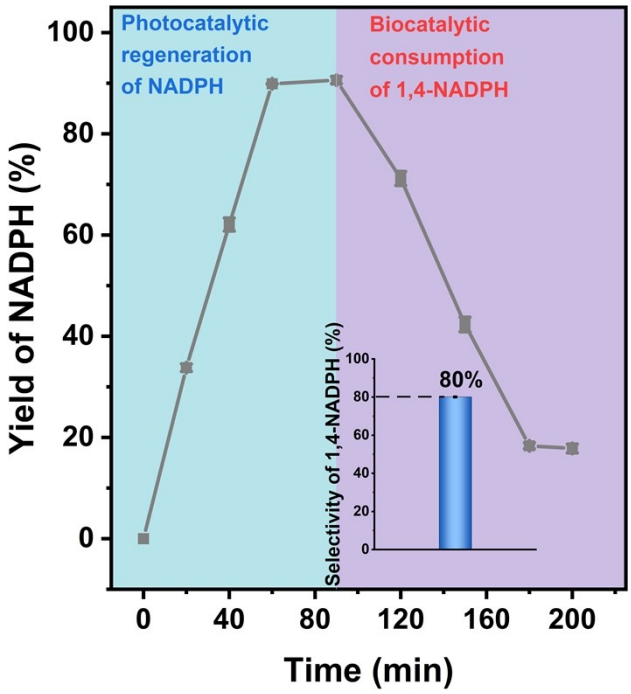

Fig. S13. NADPH yield over time (0-90 min) during photocatalytic reduction of $NADP^+$ in the presence of 0.5 M TEOA and biocatalytic consumption of 1,4-NADPH (with addition of ADH and acetaldehyde at 37 °C) against time (90-200 min). Inset in (b) shows the selectivity of 1,4-NADPH.

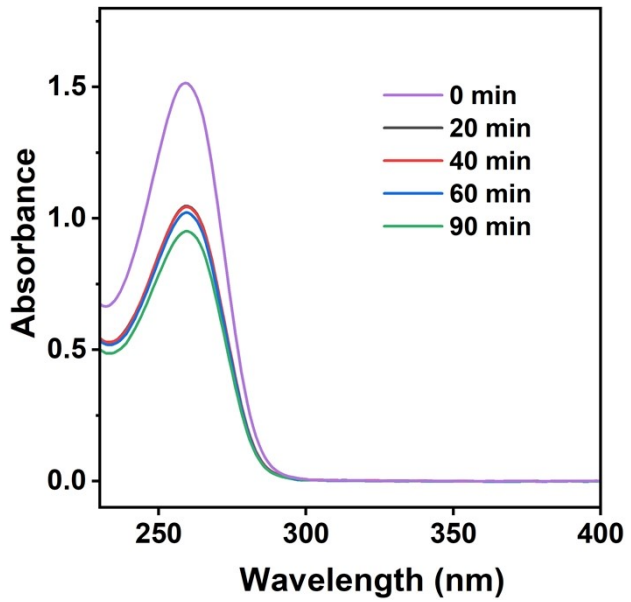

Fig. S14. UV-vis spectra of fresh NAD^+ aqueous solution and the supernatants centrifuged from in-the-dark NAD^+ adsorption by $Bi_{12}O_{17}Cl_2$-$Bi_{48}Al_2O_{75}$-Al_2O_3 at different time.

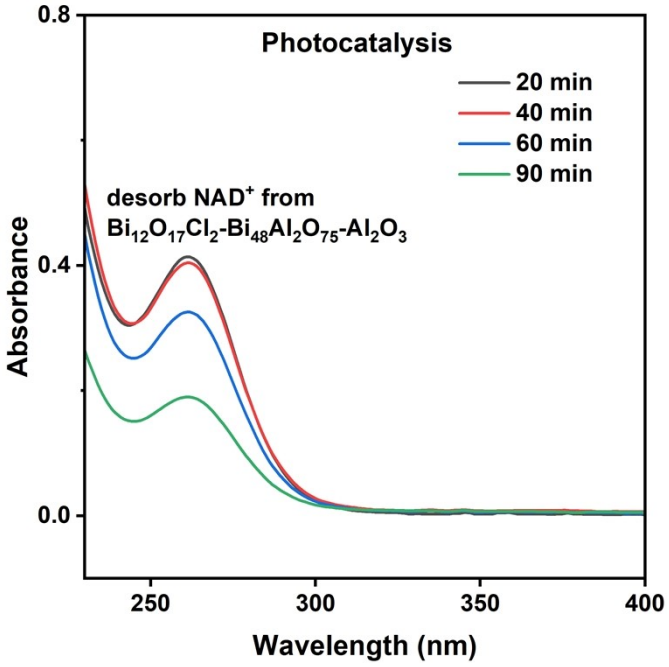

Fig. S15. UV-vis spectra of the supernatants centrifuged from NAD^+ desorption experiments after photocatalytic reduction of NAD^+ by $Bi_{12}O_{17}Cl_2$-$Bi_{48}Al_2O_{75}$-Al_2O_3 at different time.

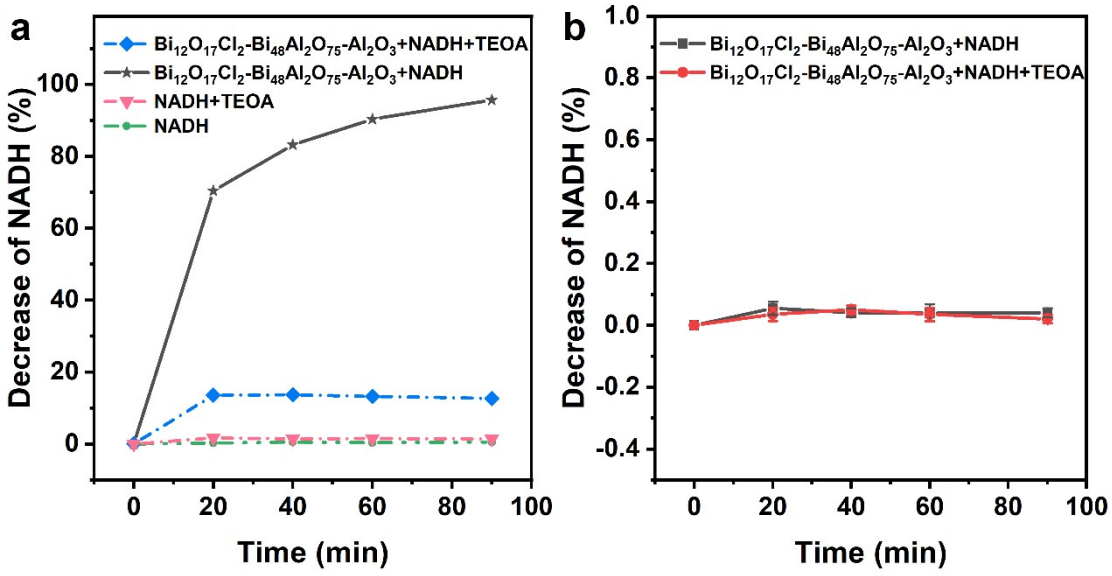

Fig. S16. (a) the stability of NADH in different conditions under lighting of 455 nm LED lamp; and (b) adsorption of NADH on $Bi_{12}O_{17}Cl_2$-$Bi_{48}Al_2O_{75}$-Al_2O_3 in aqueous solution without and with TEOA in the dark.

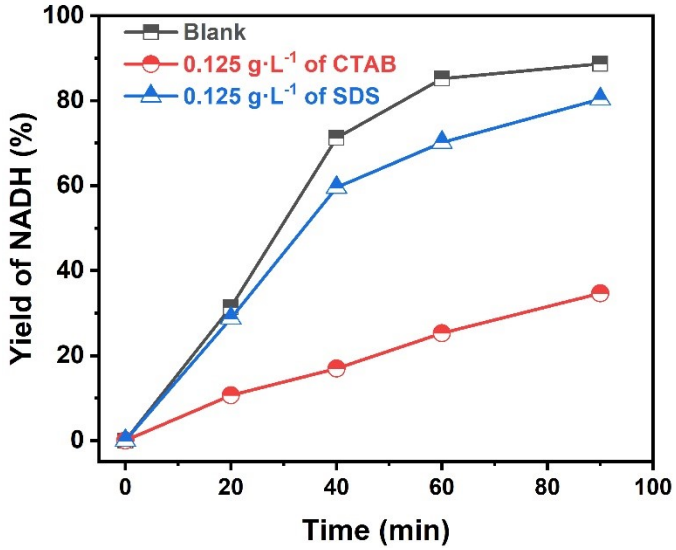

Fig. S17. The photocatalytic NADH yields at different time by 1.25 g·L^{-1} of $Bi_{12}O_{17}Cl_2$-$Bi_{48}Al_2O_{75}$-Al_2O_3 in the presence of 0.125 g·L^{-1} of CTAB and SDS.

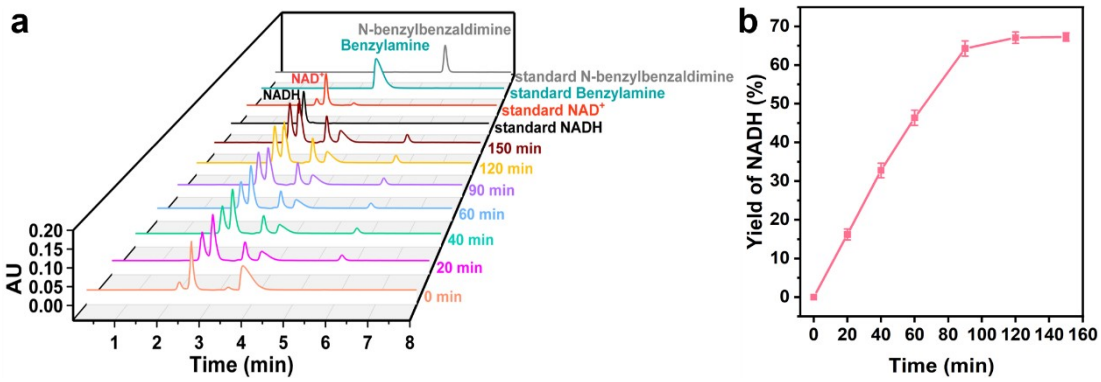

Fig. S18. (a) liquid chromatograms and (b) NADH yield at different time for the coupling of photocatalytic reduction of NAD^+ and oxidation of benzylamine by $Bi_{12}O_{17}Cl_2$-$Bi_{48}Al_2O_{75}$-Al_2O_3.

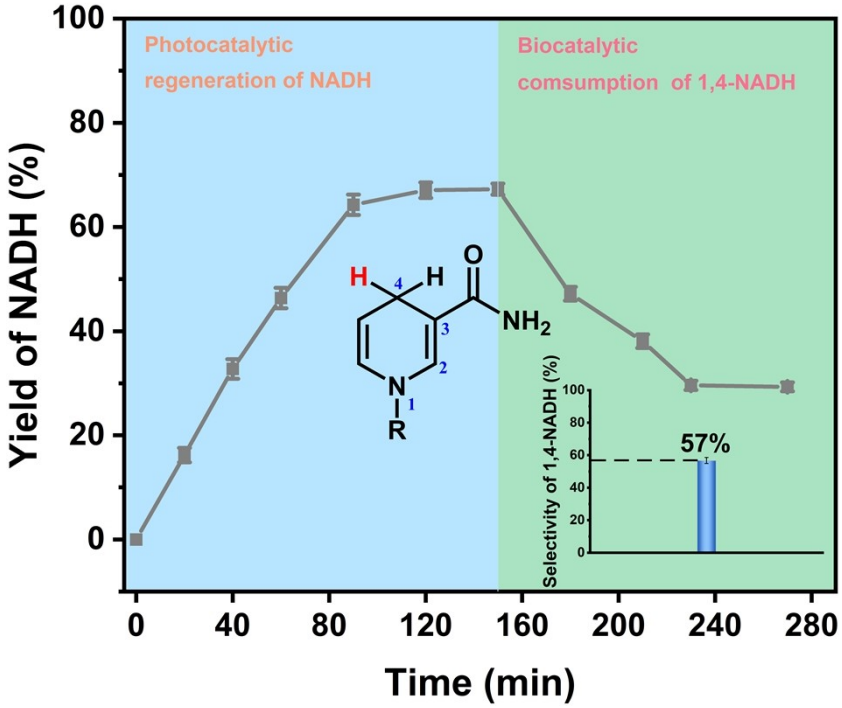

Fig. S19. NADH yields over time (0-150 min) during photocatalytic reduction of NAD^+ in the presence of 5 mM benzylamine and biocatalytic consumption of 1,4-NADH (with addition of ADH and acetaldehyde at 37 °C) against time (150-280 min). Inset shows the selectivity of 1,4-NADH.

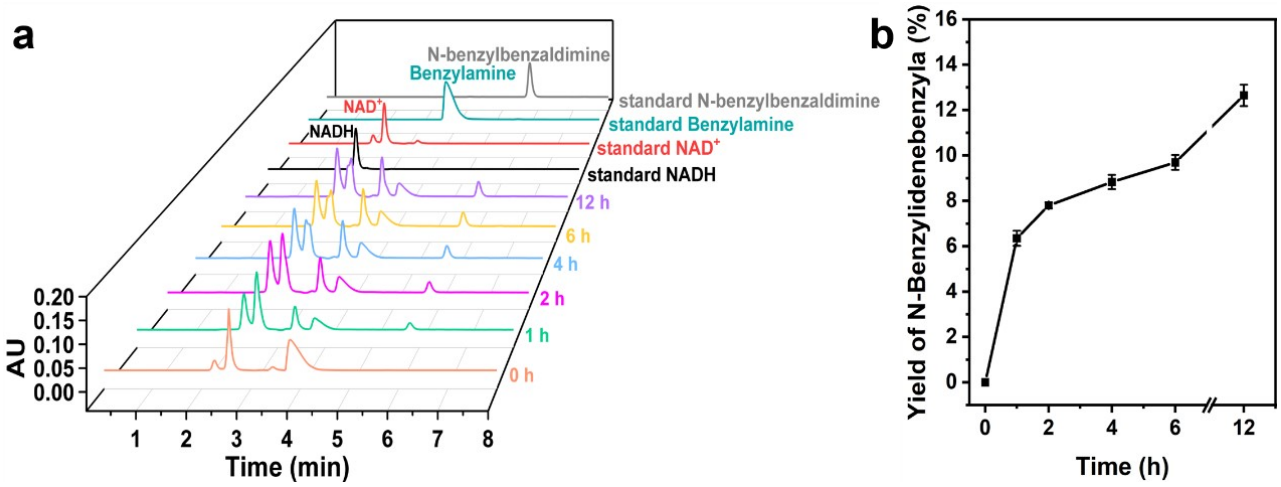

Fig. S20. (a) liquid chromatograms and (b) *N*-benzylidenebenzyla yields at different time for the coupling of photocatalytic reduction of NAD^+ and oxidation of benzylamine by $Bi_{12}O_{17}Cl_2$-$Bi_{48}Al_2O_{75}$-Al_2O_3.

Table S1 A summary of NADH yields and true biological activity of 1,4-NADH validated by enzymes in the reported photocatalytic regeneration systems.

Photocatalyst	**Electron Donor**	**Yield of NADH (%)**	**Yield of 1,4-NADH (%)**	**Light source**	**Mediator**	**Ref**
$Bi_{12}O_{17}Cl_2$-$Bi_{48}Al_2O_{75}$-Al_2O_3	TEOA, 0.5 M	89 (NADH)	68.5	455 nm LED lamp	—	*This work*
	TEOA, 0.5 M	92 (NADPH)	73.6 (1,4-NADPH)			
	Benzylamine 5 mM	67 (NADH)	38.2			
g-C_3N_4	TEOA,16 v/v%; PBS buffer, 0.1 M	40	0	80 W Xe lamp with a 400 nm cutoff filter	—	5
N,S-CDs	TEOA 0.4 M	52.3	42.92	405 nm LED lamp	—	6
	glucose or fructose	—	8			
Mesoporous g-C_3N_4	TEOA, 1 M	50	validation by enzymes	420 nm LED lamp	—	7
Au NPs	TEOA, 1 M	11.0	validation by	450 nm continuous wave	—	8

			enzymes	(CW) diode laser		
CZGO@5%Pt	TEOA, 0.75 M	74.8/80.6/83.5	validation by enzymes	In the dark (Pre-lighted the catalyst by 500 W Xe lamp with a 420 nm cutoff filter for 1 h)	—	[9]
TP-COF	TEOA,15 w/v%; PBS buffer, 0.1 M	45.5	Not measured	300 W Xe lamp with a 420 nm cutoff filter	—	[10]
Mesoporous g-C_3N_4 spheres	TEOA,15 w/v%; PBS buffer, 0.1 M	50	Not measured	420 nm LED lamp	—	[11]
Polydopamine/g-C_3N_4	TEOA,15 w/v%; PBS buffer, 0.1 M	94.7	Not measured	Xe lamp with a 420 nm cutoff filter	—	[12]
Potassium-ionized graphitic carbon nitride	TEOA, 1M; PBS buffer, 0.1 M	80	100	$\lambda > 420$ nm, visible light	0.2 mM [Cp*Rh(bpy) H_2O]$^{2+}$	[13]
Tetra(4-carboxyphenyl)	TEOA, 5 mM; PBS	81.5	29.1	330 W Xe lamp with	0.5 mM [Cp*Rh(bpy)	[14]

porphyrin (TCPP)	buffer, 0.05 M			a 400 nm cutoff filter	$H_2O]^{2+}$	
$TPTTA_5$@$TPBpy_{0.75}$-Rh/SiO_2	TEOA (15 w/v %; PBS buffer	69	validation by enzymes	λ≥ 420 nm, visible light	0.42% [Cp*Rh(bpy) $H_2O]^{2+}$	[15]
carbon nitride nanorods	TEOA, 15 w/v%; PBS buffer, 0.1 M	72	72	λ>420 nm visible light	0. 5 mM [Cp*Rh(bpy) $H_2O]^{2+}$	[16]
CdS-TiO_2 nanotubular film	TEOA,15 w/v%; PBS buffer, 0.1 M	75.2	validation by enzymes	500 W Xe lamp with a 420 nm cutoff filter	0.25 mM [Cp*Rh(bpy) $H_2O]^{2+}$	[17]
CdS-coated SiO_2	TEOA,15 w/v%; PBS buffer, 0.1 M	70.0	validation by enzymes	λ>420 nm visible light	0.25 mM [Cp*Rh(bpy) $H_2O]^{2+}$	[18]
Co/C_3N_4	TEOA,15 w/v%; PBS buffer, 0.2 M	99	validation by enzymes	450 nm LED lamp	0.25 mM [Cp*Rh(bpy) $H_2O]^{2+}$	[19]
FF/THPP/nPt	TEOA,15 w/v%; PBS buffer, 0.1 M	96	validation by enzymes	450 W Xe lamp λ>400 nm visible light	0.5 mM [Cp*Rh(bpy) $H_2O]^{2+}$	[20]
QD@Flake g-	TEOA,10	22.5	Not	500 W Xe	0.25 mM	[21]

C_3N_4	w/v%; PBS buffer, 0.1 M		measured	lamp with a 420 nm cutoff filter	[Cp*Rh(bpy)H_2O]$^{2+}$	
T-COF-2	TEOA, 0.9 M	43.8	Not measured	300 W Xe lamp with a 420 nm cutoff filter	0.3 mM [Cp*Rh(bpy)H_2O]$^{2+}$	[22]
Carbon-doped TiO_2	H_2O	63.98	Not measured	λ>400 nm visible light	0.3 mM [Cp*Rh(bpy)H_2O]$^{2+}$	[23]
Pt NPs	TEOA, 0.4 M	86	Not measured	330 W Xe lamp with a 420 nm cutoff filter	0.25 mM [Cp*Rh(bpy)H_2O]$^{2+}$	[24]

Table S2 Concentration of NAD^+ desorbed from $Bi_{12}O_{17}Cl_2$-$Bi_{48}Al_2O_{75}$-Al_2O_3 (C_{desorb}) and involved in photocatalysis ($C_{photocatalysis}$).

	20 min	40 min	60 min	90 min
C_0 (g L^{-1})	0.20	0.20	0.20	0.20
C_{desorb} (g L^{-1})	0.05	0.05	0.04	0.02
$C_{photocatalysis}$ (g L^{-1})	0.15	0.15	0.16	0.18

C_0: initial concentration of NAD^+.

C_{desorb}: the concentration of NAD^+ desorbed from $Bi_{12}O_{17}Cl_2$-$Bi_{48}Al_2O_{75}$-Al_2O_3 at different time.

$C_{photocatalysis}$ = the concentration of NAD^+ actually involved in photocatalysis at different time.

References

1. G. Kresse and J. Furthmiiller., *Comput. Mater.*, 1996, **6**, 15-50.
2. John P. Perdew, Kieron Burke and M. Ernzerhof, *Phys. Rev. Lett.*, 1996, **77**, 3865-3868.
3. P. E. Blöchl, *Phys. Rev. B*, 1994, **50**, 17953-17979.
4. H. J. Monkhorst and J. D. Pack, *Phys. Rev. B*, 1976, **13**, 5188-5192.
5. W. Jones, J. W. H. Burnett, J. F. Shi, R. F. Howe and X. D. Wang, *Joule*, 2020, **4**, 2055-2059.
6. S. S. Liu, J. F. Shi, J. S. Jia, Y. H. Yang, S. H. Zhang, D. Yang, Y. Chen, S. H. Li and Z. Y. Jiang, *ACS Catal.*, 2023, **13**, 14233-14240.
7. J. Liu and M. Antonietti, *Energy Environ. Sci.*, 2013, **6**, 1486.
8. S. Roy, V. Jain, R. K. Kashyap, A. Rao and P. P. Pillai, *Acs Catal.*, 2020, **10**, 5522-5528.
9. X. T. Yang, Z. W. Wang, X. Tan, X. Y. Yin, Y. Sun, Y. Z. Zhu and H. F. Wang, *ACS Appl. Mater. Interfaces*, 2023, **15**, 5273-5282.
10. Y. Zhao, H. Liu, C. Wu, Z. Zhang, Q. Pan, F. Hu, R. Wang, P. Li, X. Huang and Z. Li, *Angew. Chem., Int. Ed.*, 2019, **58**, 5376-5381.
11. J. Huang, M. Antonietti and J. Liu, *J. Mater. Chem. A*, 2014, **2**, 7686-7693.
12. B. B. Ma, S. Y. Sun, H. C. He, R. Lv, J. J. Deng, T. T. Huo, Y. L. Zhao, H. L. Yu and L. Zhou, *Ind. Eng. Chem. Res.*, 2019, **58**, 23567-23573.
13. Z. Xu, F. Zhou, H. Chen and J. Wang, *ACS Catal.*, 2024, 5868-5878.
14. Y. Z. Wang, J. Sun, H. H. Zhang, Z. P. Zhao and W. F. Liu, *Catal. Sci. Technol.* , 2018, **8**, 2578-2587.
15. J. Liu, X. Ren, C. Li, M. Wang, H. Li and Q. Yang, *Appl. Catal. B Environ.*, 2022, **310**, 121314.
16. J. Liu, J. H. Huang, H. Zhou and M. Antonietti, *ACS Appl. Mater. Interfaces*, 2014, **6**, 8434-8440.
17. J. Ryu, S. H. Lee, D. H. Nam and C. B. Park, *Adv. Mater.*, 2011, **23**, 1883-1888.
18. S. H. Lee, J. Ryu, D. H. Nam and C. B. Park, *Chem. Commun.* , 2011, **47**, 4643-4645.
19. W. Liu, W. Hu, L. Yang and J. Liu, *Nano Energy*, 2020, **73**, 104750.
20. J. H. Kim, M. Lee, J. S. Lee and C. B. Park, *Angew. Chem., Int. Ed.*, 2011, **51**, 517-520.
21. D. Yang, H. J. Zou, Y. Z. Wu, J. F. Shi, S. H. Zhang, X. D. Wang, P. P. Han, Z. W. Tong and Z. Y. Jiang, *Ind. Eng. Chem. Res.*, 2017, **56**, 6247-6255.
22. Y. Chen, P. Li, J. Zhou, C. T. Buru, L. Dordevic, P. Li, X. Zhang, M. M. Cetin, J. F. Stoddart, S. I. Stupp, M. R. Wasielewski and O. K. Farha, *J. Am. Chem. Soc.*, 2020, **142**, 1768-1773.
23. Y. J. Zhong, Q. L. Chen and W. Hong, *Ind. Eng. Chem. Res.*, 2005, **44**, 4165–4170.
24. S. S. Bhoware, K. Y. Kim, J. A. Kim, Q. Wu and J. Kim, *J. Phys. Chem. C*, 2011, **115**, 2553-2557.